HeartSense: Ubiquitous Accurate Multi-Modal Fusion-based Heart Rate Estimation Using Smartphones

REHAM MOHAMED, Alexandria University
MOUSTAFA YOUSSEF, Egypt-Japan Univ. of Science and Technology (E-JUST)

Heart rate is one of the most important vital signals for personal health tracking. A number of smartphone-based heart rate estimation systems have been proposed over the years. However, they either depend on special hardware sensors or suffer from the high noise due to the weakness of the heart signals, affecting their accuracy in many practical scenarios.

Inspired by medical studies about the heart motion mechanics, we propose the *HeartSense* heart rate estimation system. Specifically, we show that the gyroscope sensor is the most sensitive sensor for measuring the heart rate. To further counter noise and handle different practical scenarios, we introduce a novel quality metric that allows us to fuse the different gyroscope axes in a probabilistic framework to achieve a robust and accurate estimate.

We have implemented and evaluated our system on different Android phones. Results using 836 experiments on different subjects in practical scenarios with a side-by-side comparison with other systems show that *HeartSense* can achieve 1.03 bpm median absolute error for heart rate estimation. This is better than the state-of-the-art by more than 147% in median error, highlighting *HeartSense* promise as a ubiquitous system for medical and personal well-being applications.

CCS Concepts: •**Human-centered computing** →**Ubiquitous and mobile computing;**

General Terms: Design, Algorithms, Performance

Additional Key Words and Phrases: Heart rate detection, smartphone sensors, gyroscope, heart mechanics

ACM Reference format:
Reham Mohamed and Moustafa Youssef. 2017. HeartSense: Ubiquitous Accurate Multi-Modal Fusion-based Heart Rate Estimation Using Smartphones. *PACM Interact. Mob. Wearable Ubiquitous Technol.* 1, 3, Article 97 (September 2017), 18 pages.
DOI: http://doi.org/10.1145/3132028

1 INTRODUCTION

Recently, providing ubiquitous healthcare systems has gained momentum due to their promise in enhancing the healthcare system, personal well-being, and reducing the load on the medical infrastructure. Heart rate, i.e. how many pulses are made by the heart in one minute, is one of the main vital signals that can indicate a number of health issues [12] ranging from hypertension [13] to other diseases affecting the heart physiology such as cardiovascular diseases, heart valve disease, heart failure, tumors, or infections [1, 17, 18, 21, 27, 38, 39]. In addition, it can be used during exercising to optimize fat-burning zones and improve health and fitness [7, 25].

Typically, heart rate is measured using medical-grade devices at hospitals based on using ECG instruments or pulse oximeters. To provide more ubiquitous coverage, heart rate monitoring based on special sensors in wearables or smart phones has been introduced including chest-worn trackers [34], wristbands [24], or special hardware sensors in high-end smart phones, e.g. as in Samsung Galaxy S7. Recently, researchers have started leveraging standard cell phone sensors to measure the heart rate. One approach is to use the phone camera

DOI: http://doi.org/10.1145/3132028

to detect the changes in the fingertip color due to the different amount of oxygen in blood with heart pulses [16, 29]. Nevertheless, all these techniques do not provide accuracy in typical usage scenarios, consume high energy, and/or require special devices. A number of techniques have been proposed to measure the heart rate as a secondary signal with the breathing rate. The idea is that the periodic motion of the chest during breathing and heart pumping can be measured by the phone sensors, i.e. RF sensors [2, 3, 23, 28] or more recently inertial sensors [4] for **higher accuracy and robustness**. Different bandpass filters are used to separate the spectrum of the breathing (6-30 breath per minute (bpm)) and heart rates (54-120 beat per minute (bpm)) of the typical human. However, since the breathing motion is the dominant motion (Figure 1) that affects the human chest (due to the lungs size and their closer position to chest), heart rate estimation using mobile devices has been sensitive to noises from the surrounding or minute body motion, leading to lower accuracy in estimation.

In this paper, we present the *HeartSense* system for accurate and robust heart rate estimation using the inertial sensors of standard phone sensors. Based on medical studies of the heart mechanics that show that the heart helical shape moves spirally [6], we show that two of the gyroscope sensor axes, based on the user's pose and phone orientation; are the most sensitive to the heart motion. To work with different human poses and further tolerate noise, *HeartSense* fuses the different gyroscope axes using novel quality metrics that help it determines the best axes. *HeartSense* also proposes a Robust Lazy Heart Rate Estimator that filters the instantaneous estimates to give a robust long term heart rate estimate. By leveraging standard smart phone sensors, with the possibility of strapping the phone over the chest, *HeartSense* is suitable for several daily usage scenarios such as in emergency situations, for monitoring a patient in the convenience of his own bed, or for an athlete during exercising.

Previous work using inertial sensors to monitor the heart rate, uses the accelerometer or fuses the accelerometer and gyroscope sensors to provide an estimate for the heart rate regardless of the mechanics of the heart motion. While these systems provide the state-of-the-art accuracy [19], we show in this paper that using gyroscope axes that are more affected by heart motion gives a higher accuracy. We have implemented *HeartSense* and deployed it on a variety of Android phones. Our 836 experiments on different subjects under different realistic conditions show that *HeartSense* can achieve a median heart rate estimation error of 1.03 bpm. This is better than the state-of-the-art systems by 136%.

In summary, our contributions in this paper are four-fold:

- We present the architecture and details of a robust and accurate heart rate detection system using the inertial sensors of standard smartphones that builds on well-established studies on the mechanics of the heart motion.
- We provide novel quality metrics that capture the accuracy of each gyroscope axis under different scenarios.
- We propose a Kalman filter to fuse the different gyroscope axes.
- Finally, we present a robust estimator that combines the instantaneous heart rate estimates into a robust long term measurement.

The rest of the paper is organised as follows: We discuss a background on the mechanics of the heart motion and analysis of how it affects to the inertial sensors in Section 2. In Section 3, we show the details of *HeartSense* system. Section 4 shows the experimental evaluation. Finally, we discuss related work and conclude the paper in sections 5 and 6 respectively.

2 BACKGROUND AND SENSOR ANALYSIS STUDY

In this section, we start by a brief background about the mechanics of heart motion. We then present a study on the ability of the different inertial sensors to capture this motion with high sensitivity.

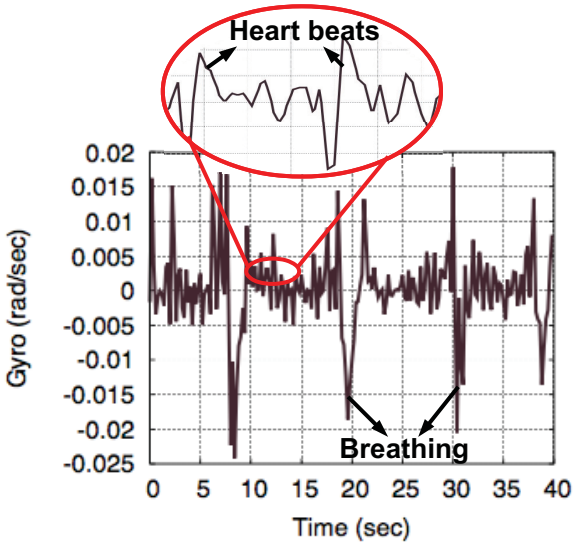

Fig. 1. Gyroscope signal with smartphone held on chest. Compared to the heart, the breathing signal is the dominant signal due to the size of the lungs and their closer position relative to the chest.

2.1 Heart Helical Motion

The heart is a muscular organ that pumps blood throughout the body, providing the body parts with the necessary oxygen and nutrients. It is located in the middle of the chest, tilted to the left. Cardiac anatomy shows that the heart has a helical structure, formed of a muscular band folded spirally [6, 26, 33, 37, 40]. Figure 2 shows the folding structure of the muscular heart band. The band is formed of two loops: a basal loop formed of a right and left segments, and an apical loop, folded to give the helical heart structure.

This helical shape causes the twisting and untwisting of the heart muscle to allow for both the suction and ejection of blood in and out of the cardiac filling [6, 26, 33, 37, 40]. This results in a wave of contractions that follows the path of the heart band as shown in Figure 3. The active contractions move along the muscular band causing narrowing of the heart underlying muscle. The sequence starts with the right segment and then goes to the left segment to cause a clockwise twisting of the heart muscle. This twisting effect further causes a counter-clockwise rotation during relaxation of the heart muscle[1].

2.2 Ability of Phone Inertial Sensors to Capture the Heart Motion

Given the heart helical motion that affects the chest accordingly, it seems natural that the gyroscope sensor should be the most sensitive sensor to detect this motion when the user places a smartphone on her chest. We performed a study to validate this intuition for different human poses (Figure 16).

Figure 4 shows an example of the captured inertial sensors signals (3-axes of the gyroscope and 3-axes of the accelerometer) in five seconds when the phone is placed **horizontally** on the chest of a **sitting** user. The actual heart rate was 90 bpm. This maps to ***7.5 heart pulses during the 5 seconds experiment***. The figure shows that the most sensitive/accurate sensors are the gyroscope X and Z axes when the phone is held horizontally. This fits the heart motion mechanics. We found that when the phone is held in a vertical position, the most affected axes

[1]A video describing the helical heart motion can be found in [8].

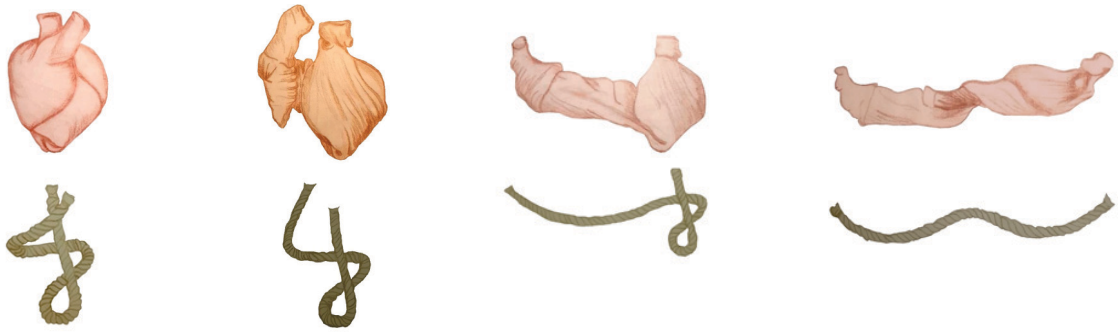

(a) The folded heart. (b) Step 1 of unfolding the heart. (c) Step 2 of unfolding the heart. (d) The unfolded heart muscle band.

Fig. 2. The heart helical structure causes the twisting and untwisting of the heart muscle to allow for both the ejection of blood and suction for cardiac filling. Analogy is shown with a rope (Figure independently redrawn. Originally from [6]).

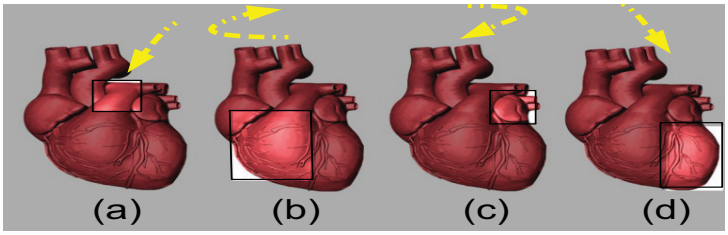

Fig. 3. Heart motion steps. The brighter parts of the heart are the currently contracted parts. The contractions move as a wave along the band, twisting the heart clockwise (Figure modified from [8]). This angular motion can be captured accurately by the phone gyroscope sensor.

are the X and Y axes, which are again aligned with the heart motion. This is maintained for different poses and phone orientations (as shown in Figure 16).

It is important to note here that ***the third gyroscope axis as well as the three accelerometer axes are very noisy***. This leads to a low accuracy in estimating the heart rate if these sensors are *blindly* used (as we quantify in Section 4). *HeartSense* builds on these findings to obtain an accurate heart rate estimate. In addition, it provides a novel quality measure for the different gyroscope axes to determine the best two axes, ***independent from the user pose or phone orientation***.

3 THE *HEARTSENSE* SYSTEM

In this section, we provide the details of *HeartSense*. We start by an overview of the system operation then provide the details of the different system components.

3.1 Overview

Figure 5 shows the *HeartSense* system architecture. *HeartSense* starts by the user holding her smartphone over the chest. As shown in Section 2, the periodic heart beats can be detected using the 3-axes gyroscope sensor: $\{\text{Gyro}_x, \text{Gyro}_y, \text{Gyro}_z\}$. These three signals are fed into the *Preprocessing Module* which reduces the noise in the

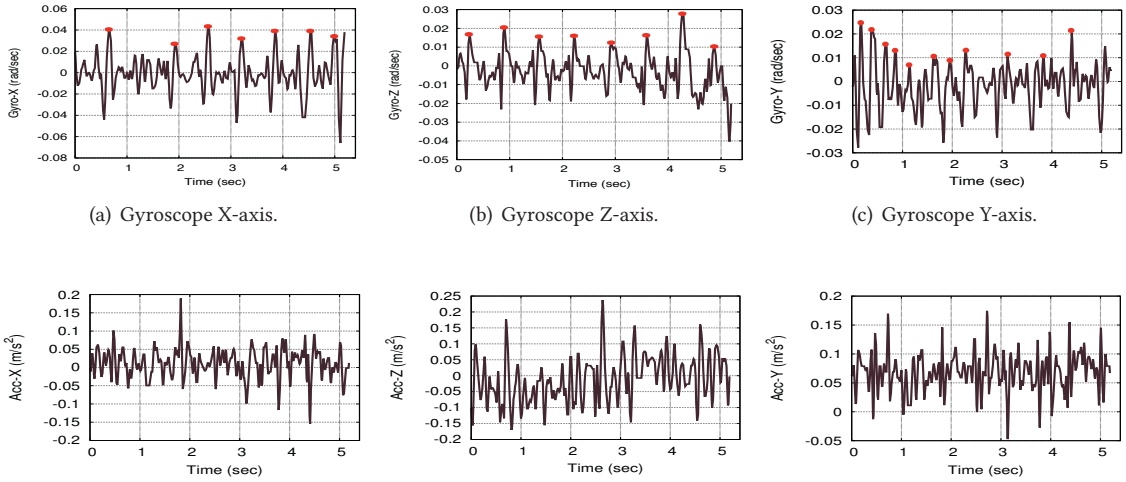

(a) Gyroscope X-axis. (b) Gyroscope Z-axis. (c) Gyroscope Y-axis.

(d) Accelerometer X-axis. (e) Accelerometer Z-axis. (f) Accelerometer Y-axis.

Fig. 4. The signal of the different inertial sensors for a phone placed horizontally over the chest of a sitting user. The ground truth heart rate is 90 bpm (**7.5 pulses in the five seconds window**). The most sensistive/accurate sensors are the gyroscope X and Z axes, fitting the heart helical motion mechanics. Other sensors and axes are significantly more noisy, leading to inaccurate estimates.

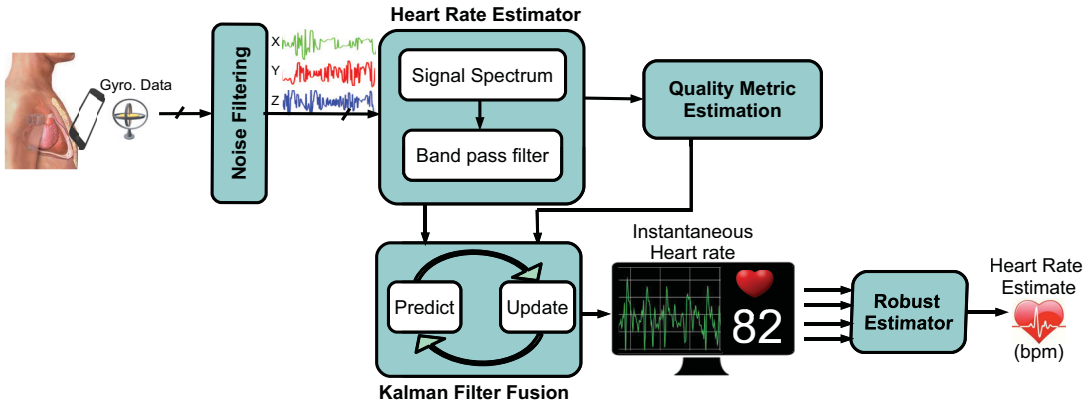

Fig. 5. *HeartSense* System Architecture.

input data. The filtered signals are then passed to the *Heart Rate Extraction Module* that estimates the heart rate from ***each axis*** signal stream as well as calculates a quality metric that reflects the confidence in each heart rate estimate of the three signals. These different estimates are then fused using a Kalman filter, taking into account the estimated quality metric for each signal. The output of the *Heart Rate Extraction Module* can be used for real-time monitoring of the heart rate. Finally, these instantaneous estimates are further post-processed by the *Robust Heart Rate Estimation Module* to remove outliers, providing a robust estimate that can be used, e.g. to log a single heart rate reading in the patient's health record.

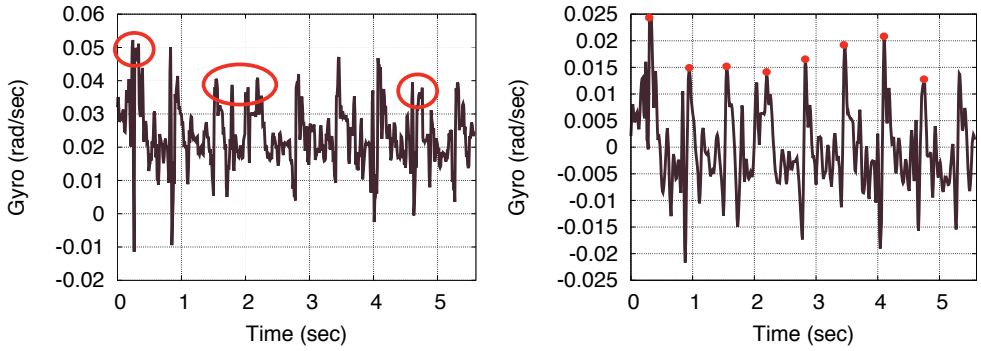

(a) Before preprocessing.

(b) After preprocessing.

Fig. 6. Effect of the local mean removal on the noisy input signal. The filter reduces noise while maintaining the heart rate pulses.

3.2 Preprocessing Module

The first task of this module is to **segment** the continuous input signals from the three gyroscope axes into fixed sliding windows of size w for processing[2].

Using sliding windows allows the system to work in realtime. After segmentation, first we remove the DC component from the signal then smooth the input signal using a *local* mean removal technique (Figure 6). Specifically, for a given gyroscope sensor axis, the smoothed signal s_j for sample j is given by:

$$s_j = \frac{1}{w_s} \sum_{i=j-\frac{w_s}{2}}^{j+\frac{w_s}{2}} (s_i - \mu) \tag{1}$$

Where w_s is the filter window size ($w_s < w$)[3], and μ is the mean of the sensor data over the entire window for DC removal.

3.3 Instantaneous Heart Rate Estimator

This is the ***main module*** of *HeartSense*. It processes the filtered signals to provide a realtime instantaneous estimate of the heart rate. It starts with estimating the heart rate from each signal individually, then fuses these estimates using a Kalman filter. For this, it calculates a novel quality metric for each sensor estimate, which reflects the accuracy of this sensor.

We first describe the details for a single sensor estimation. Then we show the quality metrics estimation and the sensors fusion to provide an instantaneous heart rate measurement.

3.3.1 Single-Sensor Heart Rate Estimation. The signals collected using the phone inertial sensors over the chest are ***usually dominated*** by the breathing motion of humans, which is remarkably stronger than the motion caused by the heart beats due to the lungs size and its relatively closer position to the chest. ***To counter/handle that***, *HeartSense* leverages two observations: **First**, the lungs motion is linear while the heart motion is helical (as shown in Section 2). **Second**: that heart and breathing rates have different ranges, where the normal heart rate

[2]We study the effect of the different parameters on system accuracy in Section 4.

[3]We experimented with different values for w_s and found that the system performance is not sensitive to w_s values $< w/40$.

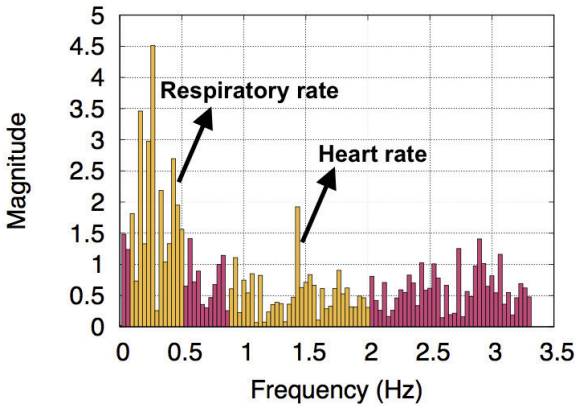

Fig. 7. The FFT of the sensor signal showing the different bands of breathing and heart rates.

ranges between 54 to 120 bpm, while the breathing rate ranges between 6 to 30 bpm [22] (Figure 7). Therefore, *HeartSense* first computes the Fast Fourier Transform (FFT) of the signal to get its spectrum. Then, it applies a bandpass filter with cutoff frequencies equal 0.9 (54 bpm) and 2 (120 bpm) to get the heart beats range. *HeartSense* then selects the frequency with maximum magnitude to estimate the current heart rate.

Formally, for a given gyroscope axis, the heart rate at time t, hr_t, is estimated as:

$$\text{hr}_t = 60 \times \underset{0.9 \le f \le 2}{\arg\max}\, \text{FFT}_t(f) \tag{2}$$

$$\text{FFT}_t(f) = \text{abs}\Big(\sum_{i=t-w}^{t} s_i \times e^{-2\pi f j/w}\Big) \tag{3}$$

Where w is the segment size from the *Preprocessing Module* and s_i is the i^{th} sample of the gyroscope s axis stream. We discuss the different values of FFT window size in Section 4.1.1.

3.3.2 Quality Metric. In typical system usage scenarios, different factors can change including the pose of the user and the orientation of the phone. This leads to changing the sensors that are the most sensitive (as shown in Section 2 and Figure 4). To address these variations and provide an accurate estimate, *HeartSense* introduces a measurement of the sensor quality that can help determine the relative confidence in the readings of three gyroscope axes.

In particular, we propose two measures of quality and compare them in Section 4. The first metric measures the *purity of the signal.* The intuition is that a perfect signal should be a sinusoidal wave with one frequency component in its spectrum that maps to the user's heart rate. To capture this, we use the kurtosis to compare the spectrum of the signal with the spectrum of a perfect sine wave. The kurtosis reflects the peakedness and tailedness of the signal: a high kurtosis distribution has a sharp peak and fatter tails, while a low kurtosis distribution has a more rounded peak and thinner tails [10]. The kurtosis quality score for the gyroscope axis s at time t, $Q_{\text{Kurt}}{}_t^s$, is defined as:

$$Q_{\text{Kurt}}{}_t^s = \frac{\text{kurt}(\text{FFT}_t^s)}{\text{kurt}(P_{\text{hr}_t^s})} \tag{4}$$

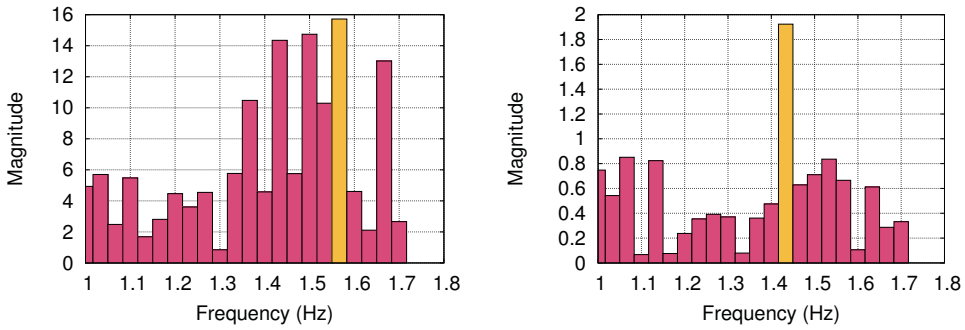

(a) Noisy signal ($Q_{\text{Kurt}} = 0.061$). (b) High-quality signal ($Q_{\text{Kurt}} = 0.185$).

Fig. 8. The FFT of a noisy and a high-quality signals with their kurtosis quality scores.

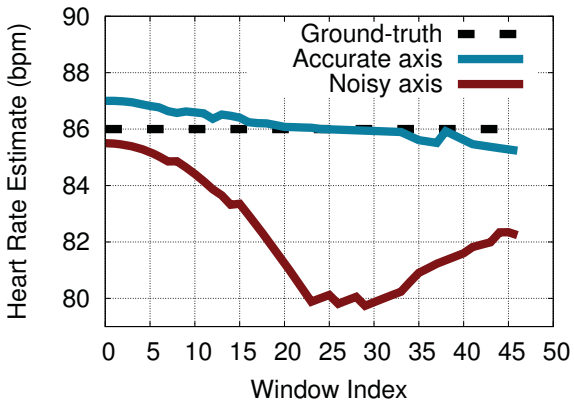

Fig. 9. The heart rate estimates of two gyroscope axes. The axis with smaller variance is more accurate.

Where $P_{\text{hr}_t^s}$ is the perfect sine wave with frequency corresponding to the estimated heart rate hr_t^s. Figure 8 shows an example of two signals spectrum with a low and high Q_{Kurt} scores.

The second metric measures the degree of ***consistency of the sensor over time***. To capture this, we measure the standard deviation of the estimate of a specific axis over time. The idea is that, if the estimates are not consistent; i.e. the standard deviation is high; this implies that the input signal is noisy. More formally, the standard deviation quality score $Q_{\text{Stdev}_t^s}$ is measured as:

$$Q_{\text{Stdev}_t^s} = \text{Stdev}(\forall_{i \in [1:t]} \text{hr}_i^s) \tag{5}$$

Figure 9 shows the heart rate estimates using two different sensor axes. The figure shows that the axis with the smaller variance gives more accurate readings.

3.3.3 Multi-Sensor Instantaneous Estimate. The final module of the *Instantaneous Heart Rate Estimator* fuses the estimates calculated from the individual gyroscope axes using a Kalman filter. The input to the Kalman filter is

the heart rate estimates from the three axes with their corresponding quality measures. The quality measures are used to model the variance of the measurement noise of the Kalman filter R. Note that in case of using kurtosis, we reverse the quality score to map to the noise variance, i.e. $R = 1 - Q_{\text{Kurt}}$.

The Kalman filter consists of two steps: The prediction and update steps. The prediction step is calculated as:

$$\bar{hr}_t = hr_{t-1} \tag{6}$$

$$\bar{P}_t = P_{t-1} + Q \tag{7}$$

Where P_t is the error variance of the estimate at time t and Q is a constant process noise variance. We start with constant values of hr_t and P_t. These values are updated over time using the Kalman filter equations. The update step is modelled as:

$$K_t = \frac{\bar{P}_t}{\bar{P}_t + R_t} \tag{8}$$

$$hr_t = \bar{hr}_t + K_t(hr_t^s - \bar{hr}_t) \tag{9}$$

$$P_t = (1 - K_t)\bar{P}_t \tag{10}$$

Where K_t is the Kalman Gain.

3.4 Robust Heart Rate Estimator

HeartSense also introduces a ***Robust Heart Rate Estimator*** to filter the instantaneous heart rate estimates to provide one robust estimate after removing the outliers. This estimate can be used, e.g. to log a reading of the heart rate in the user's medical file. This estimator uses an *α-trimmed mean filter* which orders the current samples, removes the farthest α samples from both sides of the median, then calculates the mean of the remaining samples. The α-trimmed filter has an advantage over the normal mean filter that it handles impulse noise; it also has an advantage over the median filters since it handles the Gaussian noise [5]. Specifically, the α-trimmed filter works as follows:

$$hr_R = \frac{1}{w_\alpha - \lceil 2\alpha w_\alpha \rceil} \sum_{i=\lceil \alpha w_\alpha \rceil + 1}^{w_\alpha - \lceil \alpha w_\alpha \rceil} hr_i \tag{11}$$

Where hr_R is the Robust heart rate estimate, w_α is the window size used to compute the robust estimate[4], and hr_i is the i^{th} heart rate estimate after ordering. α is a parameter that determines the type of the filter. At $\alpha = 0$, the filter mimics the standard average filter, while at $\alpha = 0.5$, the filter is equivalent to the median filter.

3.5 Discussion

HeartSense uses commodity of-the-shelf smartphones to produce accurate and reliable results. Its advantages lie in its ability to be used by any user anywhere. The user does not have to go to a hospital or visit a doctor's clinic. Also, there is no need to attach a special sensor or wear specific clothing, which is expensive or may not be available to typical users especially in developing countries. Moreover, there are no assumptions about the user's weight or chest size. *HeartSense* could be used in different scenarios: For example, a healthy user may want to regularly check her vital signs to ensure good health conditions. An athlete would also need to monitor her heart rate changes during exercising. On the other hand, a patient might want to follow the effect of a medication and avoid adverse effects. *HeartSense* could also be used in emergency cases such as falling, sudden heart attacks,

[4]We experimented with different window sizes and found that $w_\alpha = 30$ balances both accuracy and latency of the robust estimate.

Table 1. *HeartSense* system parameters.

Parameter	Range	Default value
FFT window size (w)	10 - 60 seconds	50 seconds (5000 samples)
Preprocessing window size (w_s)	0.04 - 0.5 seconds	0.04 seconds (4 samples)
Sensors in use	1, 2, 3 gyroscope axes	3 axes
Phone orientation	Vertical, Horizontal	Horizontal
Human's pose	Sitting or Lying	Sitting
Quality metric	Q_{Kurt}, Q_{Stdev}	Q_{Stdev}
α	0 - 0.5	0.1
Phone type	Samsung Note II, Samsung S5, Sony Z2	Samsung Note II

among others. Different usage scenarios have different accuracy requirements. For example, for an exercising application a relatively low accuracy may be tolerated in exchange for lower latency. On the other hand, a patient-monitoring application to confirm a certain heart condition would require high accuracy. *HeartSense* could also promote remote healthcare applications which is of paramount importance in developing countries.

HeartSense could also be used in different postures: a normal user would hold the mobile in hand on the chest while sitting to get one reading. On the contrary, a sick person might need to put the phone on her chest while lying in bed. The main usage of *HeartSense* is to obtain one accurate reading of heart rate while holding the device over the chest by hand. However, the phone could also be tied to the chest using a cheap strap (with average cost of $0.1) to allow for continuous monitoring and mobility, e.g. during exercising.

4 SYSTEM EVALUATION

We have implemented *HeartSense* and tested it on different Android devices including Samsung Note II, Samsung S5, and Sony Z2. We tested the system using 836 experiments carried on 11 persons (6 females, 5 males), with ages between 10 to 60. The subjects carried out the experiments while wearing their daily normal clothing, including heavy suits, jackets, etc. Each user carried the phone by hand over her chest in one of two phone orientations. For each orientation, experiments were done with users sitting and lying down. Data was collected during the experiments with a 100 Hz sampling rate. To collect the ground truth, we used an Omron HEM-432C blood pressure and pulse rate monitor.

Table 1 summarizes the system parameters and their default values.

4.1 Effect of System Parameters

In this section, we show the effect of the different system parameters on performance.

4.1.1 Effect of the FFT window size. Figure 10 shows the effect of changing the FFT window size (w), i.e. the segment length, on the median absolute heart rate estimation error. The figure shows that the median is not sensitive to the FFT window size. This is due to the ***low frequency*** of the heart rate signal (less than 2 Hz for the typical human range of 54-120 bpm), making a window size of 10 samples enough to reconstruct the signal.

For the rest of the paper, we set the default value of the FFT window size to 50 seconds. We note that the 50 seconds delay occurs in the initial reading only. After that, our heart rate estimator works using a sliding window with about 3 seconds offset. A 10 seconds window could be used to provide a reasonable accuracy with a lower initial latency if needed.

4.1.2 Effect of the Quality Metric. As discussed in Section 3.3.2, we propose two different quality metrics: Q_{Kurt}, which measures the purity of the FFT signal and Q_{Stdev} which measures the sensor's consistency. Figure 11

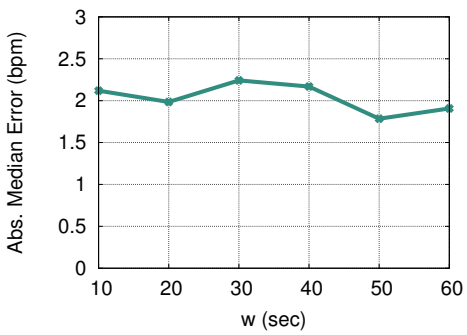

Fig. 10. Effect of the FFT window size w.

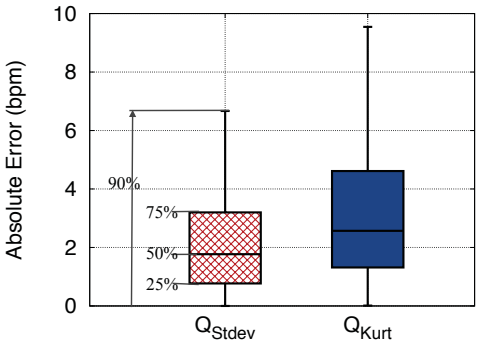

Fig. 11. Comparison between the different quality metrics.

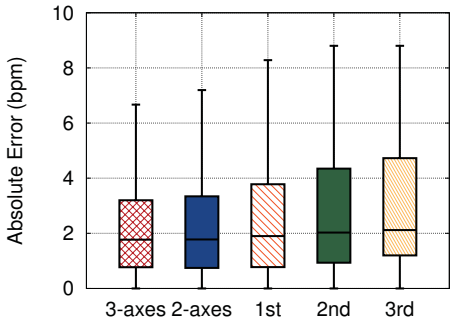

Fig. 12. Performance of using different gyroscope axes combinations ordered by the proposed quality metrics.

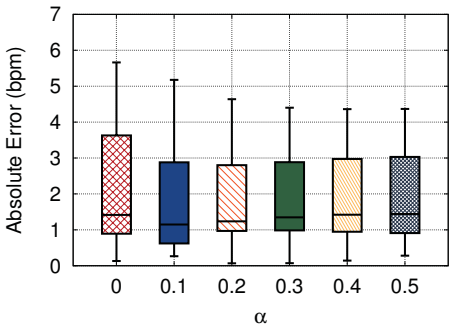

Fig. 13. Effect of α of the *Robust Estimator*.

shows the quantile plot for the two quality measures. The figure shows that the two techniques almost have the same performance error, with a slight advantage to the Q_{Stdev} technique for the extreme values.

4.1.3 Effect of Fusion of the Different Gyroscope Axes. Figure 12 shows the error of the *Instantaneous Heart Rate Estimation Module* when fusing different combinations of the gyroscope axes using the proposed quality measures in the Kalman filter. Note that when using each axis separately, the axes are ***ordered by their quality scores***. The figure shows that fusing more axes leads to better accuracy. In addition, the performance of the individual axes match the order provided by the quality metric. This highlights that the quality metric effectively captures the signal quality of the different axes.

4.1.4 Effect of α. Figure 13 shows the effect of the α value used in the α-trimmed filter by the *Robust Estimator*. At $\alpha = 0$, the filter performs as a mean filter which is more sensitive to outliers. At $\alpha = 0.5$, the filter approaches the median filter, which is not robust to the Gaussian noise. The figure shows that an optimal value can be reached at $\alpha = 0.1$.

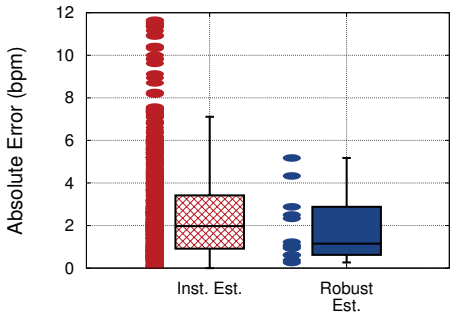

Fig. 14. Comparison between the Instantaneous and Robust Estimators of *HeartSense*.

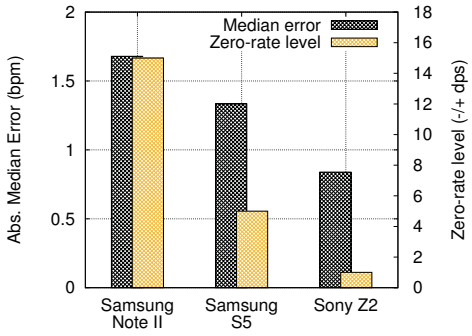

Fig. 15. Performance of *HeartSense* on different phones. The black bars show the median absolute error, while the yellow bars show the zero-rate level of the gyroscope sensor of the corresponding phone.

4.1.5 Effect of the Robust Estimator. Figure 14 compares the performance of the *Robust Estimator* to the *Instantaneous Estimator*. The figure shows that the *Robust Estimator* can enhance all the percentiles of the distribution over the *Instantaneous Estimator*, leading to a median error of less than 1.03 bpm.

4.1.6 Performance on Different Phones. In Figure 15, we show the performance of *HeartSense* on three different phones: Samsung Note II, Samsung S5, and Sony Z2. For each phone, we show the median error of heart rate estimation, as well as the zero-rate level for each phone's gyroscope chip obtained from its datasheet. The zero-rate level describes the deviation of an actual output signal from the ideal output signal if no angular change is applied. The lower the zero-rate level value, the better. The figure shows that the accuracy on a specific phone is correlated with its chip accuracy. Nevertheless, *HeartSense* error is at most 1.7 bpm in the worst case.

4.2 Overall System Performance

In this subsection, we quantify *HeartSense* overall performance. We start by showing the system performance in different scenarios. Then, we show how *HeartSense* handles different heart rates with high accuracy. Finally, we compare *HeartSense* with other approaches used in literature.

4.2.1 Performance under Different Scenarios. We evaluated *HeartSense* under different scenarios covering different human poses (sitting or lying) and different mobile orientations (vertical, horizontal). Figure 16 shows the four different combinations used in testing. Figure 17 shows the effect on the median absolute error. The figure shows the sitting pose has smaller quartile errors since the heart motion has a stronger effect on chest while sitting than sleeping. Nevertheless, *HeartSense* performance is robust to different human poses.

The figure also shows that *HeartSense* performance is robust to different orientations.

4.2.2 HeartSense Performance at Different Heart Rates. In this section, we show the different heart rates spanned by our experiments and how *HeartSense* performs with different users having different heart rates with a range between 64 to 95, including measuring ***at rest and after exercising***. Figure 18 compares between the estimated heart rate values and the actual heart rate values. The figure shows that *HeartSense* can detect the different heart rates effectively with a median error of 1.03 bpm. As the heart rate increases, the performance of *HeartSense* becomes better, where the percentage of the error at smaller range (65-75 bpm) is 3.4% while for

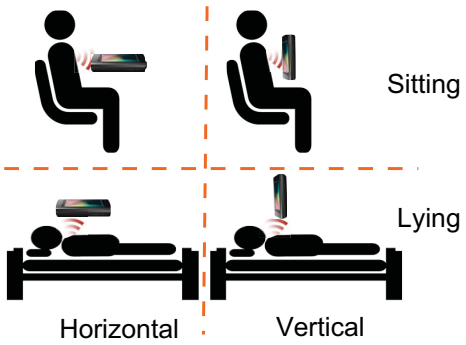

Fig. 16. Different combinations of human poses and mobile orientations used in evaluating *HeartSense*.

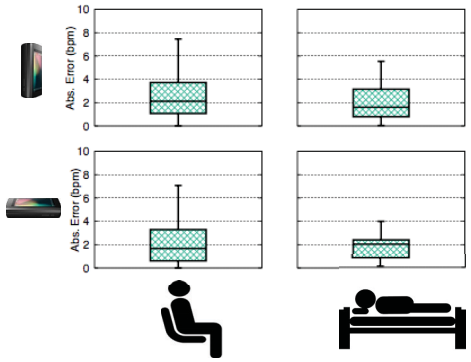

Fig. 17. Effect of the phone orientation and human pose.

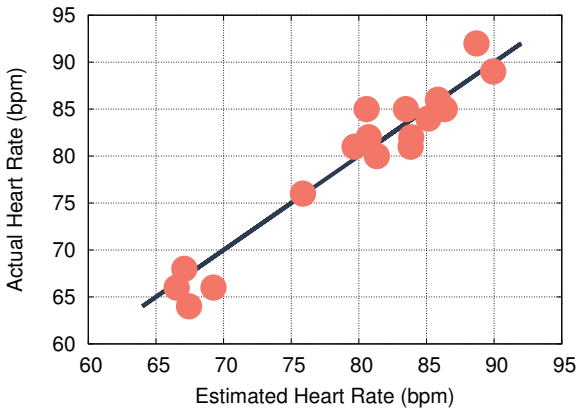

Fig. 18. Performance of *HeartSense* at different heart rates. A perfect estimate should lie on the line with slope= 1.

higher range (85-95 bpm) is 0.76%. This is due to the higher power of the heart at higher heart rates, leading to a cleaner signal on the gyroscope axes.

4.2.3 Comparison with Other Systems. Finally, we compare the performance of *HeartSense* to those that use the standard phone sensors. Since the inertial sensors (e.g. [14]) in general are more accurate than RF-based systems (e.g. [2, 23]) due to their closer distance to the heart, we use the state-of-the-art inertial-based system [14] for comparison. Furthermore, we also compare *HeartSense* performance to two of the popular commercial Android applications: One that uses the special heart rate sensor on **high-end smart phones** [32] and another that uses the built-in camera for measuring the heart rate by tracking the color change of the fingertip [15]. The applications have more than 25 million downloads and their average rating is more than 4.3.

Figure 19(a) shows the CDF of error and Table 2 summarizes the results. The results show that *HeartSense* significantly outperforms the accelerometer-based systems by more than 385% in median error. More interestingly, *fusing the accelerometer with the gyroscope* axes using the weighting metrics introduced in Section 3 ***leads to worse*** performance compared to using the gyroscope alone (as in *HeartSense*) due to the high noise of the

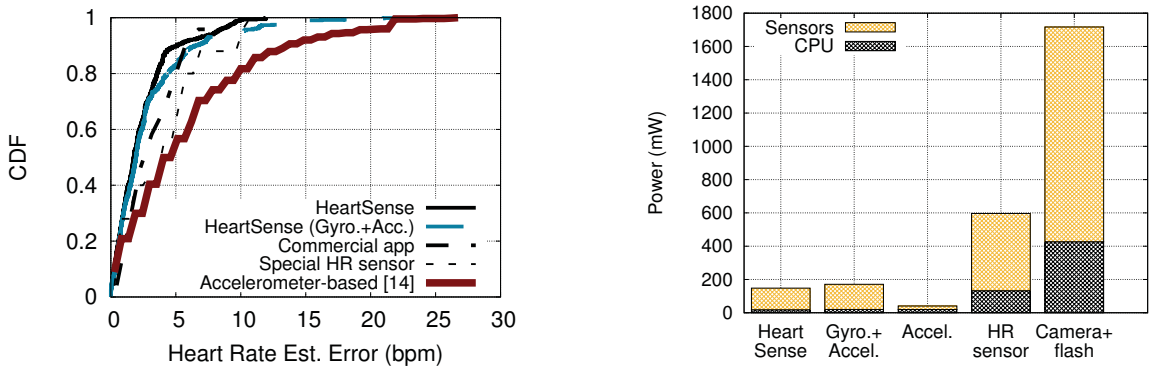

(a) (b)

Fig. 19. Comparison between *HeartSense* and the state-of-the-art [14] and two highly-downloaded applications from the application store that use the camera and the special heart sensor on high-end devices [15, 32]. (a) CDF of the error. (b) Power Consumption.

Table 2. Summary of the comparison between *HeartSense* and the state-of-the-art system in [14] and two highly popular applications from the application store that use the camera and the special heart sensor on high-end devices. The numbers in the table represent the absolute error. **Numbers between parenthesis** represent the percentage of degradation compared to *HeartSense*.

	HeartSense	***HeartSense* (Gyro.+Accel.)**	**Accelerometer-based [14]**	**Commercial App (Special HR sensor) [32]**	**Commercial App (Camera) [15]**
25th perc.	0.38	0.79 (107.9%)	2 (426.3%)	1 (255.3%)	0.83 (117.1%)
50th perc.	1.03	1.92 (86.4%)	5 (385.4%)	2.55 (147.6%)	3.85 (273.8%)
75th perc.	3.59	3.77 (5.01%)	9 (150.7%)	4.64 (29.2%)	5.54 (54.3%)
RMSE	4.98	5.18	8.28	4.07	5.2
Power (mW)	148.05	170.92	40.46	596.6	1716.8

accelerometer sensor. This ***confirms our findings*** throughout the paper and highlights the ability of *HeartSense* to provide ubiquitous, accurate, and robust heart rate estimation using standard cell phones. The figure also shows that *HeartSense* outperforms the commercial applications that use the built-in camera or the special hardware sensor by more than 147%. This is due to the high sensitivity of both techniques to the placement of the finger over the camera/sensor. It is important also to note that using the camera and turning on the flash (required for both the special heart rate sensor and camera-based techniques) can drain the scarce phone battery quickly, compared to using the energy-efficient inertial sensors. Figure 19(b) shows the power consumption of *HeartSense* compared to the other systems, we calculated the CPU power consumption using the PowerTutor profiler [41] and the sensors datasheets.

5 RELATED WORK

In this section, we discuss the work related to *HeartSense*. We start with showing the systems that use the smartphones to measure different vital signs other than the heart rate. Then, we discuss related work that measure the heart rate in particular.

5.1 Measuring Vital Signs using Smartphones

Over the years, smartphones have been used for different healthcare purposes including breathing rate monitoring [2, 23], blood pressure [30], colorimetric diagnostic assays [35], newborn jaundice [9], and lung functions [20]. UbiBreathe [2] uses the RSS of standard WiFi equipment to estimate the breathing rate and detect apnea. In [23], authors extend the idea to use the more detailed CSI information. Zephyr [4] uses different inertial sensors to detect the motion of the chest caused by breathing, leading to more accurate and robust estimates.

SpiroSmart [20] uses the phone microphone to measure the lung function. The idea is for user to breathe in their full lung volume and forcefully exhale back at the phone. The sound is processed to detect the flow rate.

To measure the blood pressure, [30] combines an external microphone or a second phone with the built-in camera by computing the pulse pressure and the stroke volume from the sensors data. The phone camera has also been used for colorimetric diagnostic assays [35] and newborn jaundice [9], which use calibration techniques to compensate for measurement errors due to the variability in ambient light.

HeartSense complements these systems by providing accurate and robust heart rate detection using the gyroscope sensor in standard smartphones based on studying the heart motion mechanics.

5.2 Heart Rate Detection

Heart rate is typically measured in medical facilitates using special devices such as the electrocardiogram (ECG) instruments or pulse oximeters. The former depends on measuring the electrical impulses of the heart while the latter depends on analyzing the difference in light absorbtion of red and infrared light. This requires special devices to be ***inconveniently*** attached to the person's body. In addition, the ***cost*** may be prohibitive in many situations.

To provide ubiquitous heart rate estimation, other systems use wearable accelerometer sensors [11, 19, 34, 36] attached to the body to monitor the heart rate. However, this requires **special hardware** and, as shown in the experiment section, the accelerometer sensor is **less sensitive** to the heart motion mechanics as compared to the gyroscope sensor. BioPhone [14] also uses smartphone accelerometer to measure the heart rate in different static postures. However, it aggregates the three sensors axes without rating, unlike *HeartSense*, which fuses the axes of the gyroscope using a Kalman filter by accurately measuring the variance of the measurement noise using our quality metrics, therefore, it provides higher accuracy.

To provide a non-invasive solution, researchers have proposed using RF signals for estimating the heart rate [3, 28, 31]. The idea is that an RF signal going through the chest will be affected by the periodic motion of the body parts (mainly the lungs and heart as **a secondary signal**). This motion can be captured by RF sensors. For example, in [28], the authors use a dense array of wireless sensor nodes to estimate the breathing and heart rate. The system in [3] uses special directed antennae to focus the signal on the human body and detect the heart rate based on the periodic change in the phase of the received signal. Similarly, DopplerSleep [31] which analyzes the sleeping behaviour by measuring different vital signs, including the heart rate, using a doppler radar. Although these techniques provide reasonable accuracy, usually in controlled environments, they still require special hardware, which raises ***cost and scalability*** issues.

More recently, a number of techniques that leverage the standard phone sensors for estimating the heart rate have been proposed [2, 4, 16, 23, 29]. In [16, 29] use the phone camera and flash to estimate the breathing rate by analyzing the blood color change with the heart pulses, similar to the oximeter principle. Similarly, some cellular manufacturers, e.g. in high-end Samsung phones, include a special sensor for measuring the heart rate using the same idea. However, using the phone camera leads to limited unreliable accuracy and a special sensor is not a scalable solution. Other techniques use the standard WiFi RSS or CSI information, e.g. [2, 23], to estimate the heart rate; similar to RF techniques that use special sensors. However, using standard WiFi signals leads to limited accuracy in many practical scenarios and requires the phone to be close to the AP. Zypher [4] leverages

the inertial phone sensors to estimate the ***breathing rate only*** by placing the phone on the chest and suggest estimating the heart rate by using a bandpass filter. It can provide good accuracy in breathing rate estimation as compared to RF-based techniques. However, as we ***quantified*** in the evaluation section, using the accelerometer sensor for heart rate estimation is not reliable.

HeartSense, on the other hand, builds on well-established studies in the medical domain to remove low-quality sensors, leading to better accuracy and robustness using standard cell phones. In addition, it combines different modules to handle the noise and variations of the typical usage scenarios.

6 CONCLUSION

We presented the design and implementation of *HeartSense*: an accurate and robust system for ubiquitous heart rate detection. *HeartSense* uses the commodity off-the-shelf smart phones to measure human's heart rate using the gyroscope sensors. Inspired by medical studies of the mechanics of the heart motion, we showed that the gyroscope sensor is the most sensitive to capture the spiral heart movement. We further presented two quality metrics that can weigh the quality of the different gyroscope axes independent of the human pose or phone orientation. A Kalman filter is proposed to the estimates from the different axes to obtain an accurate real-time heart rate estimate. This instantaneous estimate is further post-processed to remove outliers and provide robust heart rate measurements.

Evaluation of *HeartSense* using 836 experiments on different subjects shows that it can achieve a median absolute error of 1.03 bpm under different practical scenarios. This is better than the state-of-the-art commercial smartphone applications by more than 136%.

Currently, we are extending *HeartSense* in different directions including detecting abnormalities in the heart signal, estimating other vital signals, among others.

REFERENCES

[1] Ahmed H Abdelhafiz. 2002. Heart failure in older people: causes, diagnosis and treatment. *Age and ageing* 31, 1 (2002), 29–36.

[2] Heba Abdelnasser, Khaled A Harras, and Moustafa Youssef. 2015. UbiBreathe: A ubiquitous non-invasive WiFi-based breathing estimator. In *Proceedings of the 16th ACM International Symposium on Mobile Ad Hoc Networking and Computing*. ACM, 277–286.

[3] Fadel Adib, Hongzi Mao, Zachary Kabelac, Dina Katabi, and Robert C Miller. 2015. Smart homes that monitor breathing and heart rate. In *Proceedings of the 33rd Annual ACM Conference on Human Factors in Computing Systems*. ACM, 837–846.

[4] Heba Aly and Moustafa Youssef. 2016. Zephyr: Ubiquitous Accurate multi-Sensor Fusion-based Respiratory Rate Estimation Using Smartphones. In *Proceedings of IEEE Conference on Computer Communications (INFOCOM)*.

[5] J Bednar and T Watt. 1984. Alpha-trimmed means and their relationship to median filters. *IEEE Transactions on acoustics, speech, and signal processing* 32, 1 (1984), 145–153.

[6] Gerald D Buckberg. 2002. Basic science review: the helix and the heart. *The Journal of Thoracic and Cardiovascular Surgery* 124, 5 (2002), 863–883.

[7] Daniel G Carey. 2009. Quantifying differences in the fat burning zone and the aerobic zone: implications for training. *The Journal of Strength & Conditioning Research* 23, 7 (2009), 2090–2095.

[8] The Helical Heart Company. 2005. The helical heart. http://www.helicalheart.com/video_center.htm. (2005). [Online. Last accessed 14-Feb-2017].

[9] Lilian De Greef, Mayank Goel, Min Joon Seo, Eric C Larson, James W Stout, James A Taylor, and Shwetak N Patel. 2014. Bilicam: using mobile phones to monitor newborn jaundice. In *Proceedings of the 2014 ACM International Joint Conference on Pervasive and Ubiquitous Computing*. ACM, 331–342.

[10] Lawrence T DeCarlo. 1997. On the meaning and use of kurtosis. *Psychological methods* 2, 3 (1997), 292.

[11] M Di Rienzo, E Vaini, P Castiglioni, G Merati, P Meriggi, G Parati, A Faini, and F Rizzo. 2013. Wearable seismocardiography: Towards a beat-by-beat assessment of cardiac mechanics in ambulant subjects. *Autonomic Neuroscience* 178, 1 (2013), 50–59.

[12] Malcolm Elliott and Alysia Coventry. 2012. Critical care: the eight vital signs of patient monitoring. *Br J Nurs* 21, 10 (2012), 621–625.

[13] Matthew W Gillman, William B Kannel, Albert Belanger, and Ralph B D'Agostino. 1993. Influence of heart rate on mortality among persons with hypertension: the Framingham Study. *American heart journal* 125, 4 (1993), 1148–1154.

[14] Javier Hernandez, Daniel J McDuff, and Rosalind W Picard. 2015. Biophone: Physiology monitoring from peripheral smartphone motions. In *Engineering in Medicine and Biology Society (EMBC), 2015 37th Annual International Conference of the IEEE*. IEEE, 7180–7183.

[15] Azumio Inc. 2010. Instant Heart Rate [Mobile application software]. (2010). Retrieved from https://play.google.com.
[16] E Jonathan and Martin Leahy. 2010. Investigating a smartphone imaging unit for photoplethysmography. *Physiological measurement* 31, 11 (2010), N79.
[17] C Omar F Kamlin, Colm PF O'Donnell, Neil J Everest, Peter G Davis, and Colin J Morley. 2006. Accuracy of clinical assessment of infant heart rate in the delivery room. *Resuscitation* 71, 3 (2006), 319–321.
[18] William B Kannel, Craig Kannel, Ralph S Paffenbarger, and L Adrienne Cupples. 1987. Heart rate and cardiovascular mortality: the Framingham Study. *American heart journal* 113, 6 (1987), 1489–1494.
[19] Federica Landreani, Alba Martin-Yebra, Claudia Casellato, Esteban Pavan, Carlo Frigo, Pierre-François Migeotte, and Enrico G Caiani. 2015. Feasibility study for beat-to-beat heart rate detection by smartphone's accelerometers. In *E-Health and Bioengineering Conference (EHB), 2015*. IEEE, 1–4.
[20] Eric C Larson, Mayank Goel, Gaetano Boriello, Sonya Heltshe, Margaret Rosenfeld, and Shwetak N Patel. 2012. SpiroSmart: using a microphone to measure lung function on a mobile phone. In *Proceedings of the 2012 ACM Conference on Ubiquitous Computing*. ACM, 280–289.
[21] Albert B Levin. 1966. A simple test of cardiac function based upon the heart rate changes induced by the Valsalva maneuver. *The American journal of cardiology* 18, 1 (1966), 90–99.
[22] Wilburta Q Lindh, Marilyn Pooler, Carol D Tamparo, Barbara M Dahl, and Julie Morris. 2013. *Delmar's comprehensive medical assisting: administrative and clinical competencies*. Cengage Learning.
[23] Jian Liu, Yan Wang, Yingying Chen, Jie Yang, Xu Chen, and Jerry Cheng. 2015. Tracking vital signs during sleep leveraging off-the-shelf wifi. In *Proceedings of the 16th ACM International Symposium on Mobile Ad Hoc Networking and Computing*. ACM, 267–276.
[24] NH Mahmood, N Uyop, N Zulkarnain, FK Che Harun, MF Kamarudin, and A Linoby. 2011. LED indicator for heart rate monitoring system in sport application. In *Signal Processing and its Applications (CSPA), 2011 IEEE 7th International Colloquium on*. IEEE, 64–66.
[25] Alison M McManus, Rich SW Masters, Raija MT Laukkanen, CW Clare, Cindy HP Sit, and Fiona CM Ling. 2008. Using heart-rate feedback to increase physical activity in children. *Preventive medicine* 47, 4 (2008), 402–408.
[26] Satoshi Nakatani. 2011. Left ventricular rotation and twist: why should we learn? *Journal of Cardiovascular Ultrasound* 19, 1 (2011).
[27] Alexandros Pantelopoulos and Nikolaos G Bourbakis. 2010. Prognosis: a wearable health-monitoring system for people at risk: Methodology and modeling. *IEEE Transactions on Information Technology in Biomedicine* 14, 3 (2010), 613–621.
[28] N. Patwari, L. Brewer, Q. Tate, O. Kaltiokallio, and M. Bocca. 2014. Breathfinding: A Wireless Network That Monitors and Locates Breathing in a Home. *IEEE Journal of Selected Topics in Signal Processing* 8, 1 (2014), 30–42.
[29] Panagiotis Pelegris, K Banitsas, T Orbach, and Kostas Marias. 2010. A novel method to detect heart beat rate using a mobile phone. In *2010 Annual International Conference of the IEEE Engineering in Medicine and Biology*. IEEE, 5488–5491.
[30] Rong-Chao Peng, Wen-Rong Yan, Ning-Ling Zhang, Wan-Hua Lin, Xiao-Lin Zhou, and Yuan-Ting Zhang. 2015. Cuffless and Continuous Blood Pressure Estimation from the Heart Sound Signals. *Sensors* 15, 9 (2015), 23653–23666.
[31] Tauhidur Rahman, Alexander T Adams, Ruth Vinisha Ravichandran, Mi Zhang, Shwetak N Patel, Julie A Kientz, and Tanzeem Choudhury. 2015. Dopplesleep: A contactless unobtrusive sleep sensing system using short-range doppler radar. In *Proceedings of the 2015 ACM International Joint Conference on Pervasive and Ubiquitous Computing*. ACM, 39–50.
[32] Ltd. Samsung Electronics Co. 2014. Samsung Health [Mobile application software]. (2014). Retrieved from https://play.google.com.
[33] Partho P Sengupta, A Jamil Tajik, Krishnaswamy Chandrasekaran, and Bijoy K Khandheria. 2008. Twist mechanics of the left ventricle: principles and application. *Journal of the American College of Cardiology* 1, 3 (2008), 366–376.
[34] Ghufran Shafiq and Kalyana C Veluvolu. 2014. Surface chest motion decomposition for cardiovascular monitoring. *Scientific reports* 4 (2014).
[35] Li Shen, Joshua A Hagen, and Ian Papautsky. 2012. Point-of-care colorimetric detection with a smartphone. *Lab on a Chip* 12, 21 (2012), 4240–4243.
[36] AF Silva, JP Carmo, PM Mendes, and JH Correia. 2011. Simultaneous cardiac and respiratory frequency measurement based on a single fiber Bragg grating sensor. *Measurement Science and Technology* 22, 7 (2011), 075801.
[37] Francisco Torrent-Guasp, Mladen J. Kocica, Antonio F. Corno, Masashi Komeda, Francesc Carreras-Costa, A. Flotats, Juan Cosin-Aguillar, and Han Wen. 2005. Towards new understanding of the heart structure and function. *Eurpean Journal of Cardiothoracic Surgery* 27, 2 (2005), 191–201.
[38] Aly Waninge, Annette AJ Van der Putten, Roy E Stewart, Bert Steenbergen, Ruud Van Wijck, and Cees P Van der Schans. 2013. Heart rate and physical activity patterns in persons with profound intellectual and multiple disabilities. *The Journal of Strength & Conditioning Research* 27, 11 (2013), 3150–3158.
[39] Goya Wannamethee, A Gerald Shaper, and Peter W Macfarlane. 1993. Heart rate, physical activity, and mortality from cancer and other noncardiovascular diseases. *American journal of epidemiology* 137, 7 (1993), 735–748.
[40] Hongjiang Wei, Magalie Viallon, Benedicte MA Delattre, Kevin Moulin, Feng Yang, Pierre Croisille, and Yuemin Zhu. 2015. Free-breathing diffusion tensor imaging and tractography of the human heart in healthy volunteers using wavelet-based image fusion. *IEEE transactions on medical imaging* 34, 1 (2015), 306–316.

[41] Lide Zhang, Birjodh Tiwana, Robert P Dick, Zhiyun Qian, Z Morley Mao, Zhaoguang Wang, and Lei Yang. 2010. Accurate online power estimation and automatic battery behavior based power model generation for smartphones. In *Hardware/Software Codesign and System Synthesis (CODES+ ISSS), 2010 IEEE/ACM/IFIP International Conference on*. IEEE, 105–114.

Received February 2017; revised May 2017; accepted June 2017